

Disentangling Disentangled Representations: Towards Improved Latent Units via Diffusion Models

Youngjun Jun Jiwoo Park Kyobin Choo Tae Eun Choi Seong Jae Hwang*
Yonsei University

{youngjun, wldn1677, chu, teunchoi, seongjae}@yonsei.ac.kr

Abstract

Disentangled representation learning (DRL) aims to break down observed data into core intrinsic factors for a profound understanding of the data. In real-world scenarios, manually defining and labeling these factors are non-trivial, making unsupervised methods attractive. Recently, there have been limited explorations of utilizing diffusion models (DMs), which are already mainstream in generative modeling, for unsupervised DRL. They implement their own inductive bias to ensure that each latent unit input to the DM expresses only one distinct factor. In this context, we design **Dynamic Gaussian Anchoring** to enforce attribute-separated latent units for more interpretable DRL. This unconventional inductive bias explicitly delineates the decision boundaries between attributes while also promoting the independence among latent units. Additionally, we also propose **Skip Dropout** technique, which easily modifies the denoising U-Net to be more DRL-friendly, addressing its uncooperative nature with the disentangling feature extractor. Our methods, which carefully consider the latent unit semantics and the distinct DM structure, enhance the practicality of DM-based disentangled representations, demonstrating state-of-the-art disentanglement performance on both synthetic and real data, as well as advantages in downstream tasks.

1. Introduction

Disentangled representation learning (DRL) aims to uncover the fundamental factors within the observed data [3, 21, 22, 48]. A disentangled representation is a set of latent units where each unit is dependent on only one factor and invariant to the remaining factors [3, 35, 36, 44, 63]. Attaining such representation is essential for understanding data and generalizing models, making it a fundamental goal in the machine learning field [3, 43].

To achieve DRL, supervised methods that require annota-

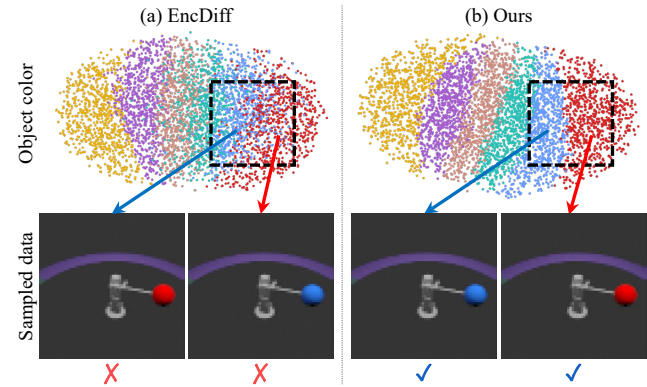


Figure 1. Visualization of latent units in EncDiff and Ours. The top figures visualize the latent unit representing object color using the dimensionality reduction method PaCMAP [26] for multiple data points. The bottom figures show the results of conditional generation of data by sampling the latent unit from the blue and red regions, respectively. (a) In EncDiff [67], the boundary between color regions is ambiguous, so a latent unit representing red can be sampled even in the blue region, and vice versa. (b) Using our proposed method, we achieve an interpretable latent unit by clearly defining the boundaries between attributes, ensuring that only one color appears in each color region.

tions of manually-defined factors have been attempted [4, 57]. However, in the real world, factors are complex and exist on a non-discrete spectrum (e.g., image brightness), making annotation challenging. Thus, unsupervised learning methods are extensively being explored [16, 48, 66]. They commonly utilize the latent space of generative models, which capture the semantic information of images. Meanwhile, it is known that achieving disentanglement in an unsupervised manner is impossible without explicit inductive biases [39], such as regularization for statistical independence and architectural modeling [25, 48, 69]. Thus, the essence of unsupervised DRL lies in how effectively a suitable inductive bias is implemented into the target generative model.

Recently, diffusion models (DMs) [23, 29, 51] have emerged as a cornerstone of generative models, known for

*Corresponding author

Project Page: <https://youngjun-jun.github.io/dis-dis-rep>

their superior generation quality and stability. In particular, DMs not only effectively encode rich information about the input image, but also ensure that the manipulated features in the latent space are directly reflected in the generated image [34]. This suggests that DMs are attractive target generative models for unsupervised DRL [66, 67, 69]. Naturally, existing DM-based DRL methods focus on providing appropriate inductive biases to DMs to achieve independence among latent units [66, 69]. Meanwhile, the significance of each latent unit accurately reflecting its corresponding factor has not yet been considered. Therefore, to enhance the practical usefulness and interpretability of representations, we not only focus on the independence of the factors (*e.g.*, `object_color`) represented by the latent units, but also on how faithfully each latent unit reflects the attributes (*e.g.*, `red`, `blue`) of those factors.

To understand this, let us consider a scenario highlighting the necessity of attribute-separated latent units. Fig. 1 visualizes a single latent unit (responsible for `object_color`) across multiple data points using both the DM-based state-of-the-art (SOTA) DRL method EncDiff [67] and our proposed method. In Fig. 1a, the data points for EncDiff are not clearly separated into distinct attributes (*e.g.*, `red`, `blue`). This entanglement might actually result in selecting a `blue` image when sampling from the `red` region. Such representation with semantically ambiguous latent units cannot guarantee the intended downstream uses (*e.g.*, manipulating `object_color` factor of intended color). In contrast, as shown in Fig. 1b, ours exhibits clear decision boundaries between attributes, ensuring that images sampled from each color region faithfully reflect the intended color. This enhances interpretability by indicating which intrinsic factor a latent unit represents in real-world data where labels are absent, suggesting a more practical representation. Moreover, latent units with a high association (*i.e.*, mutual information) with a specific factor naturally become less dependent on other factors, thereby promoting disentanglement.

Thus, we first propose **Dynamic Gaussian Anchoring (DyGA)**, an inductive bias that clarifies the decision boundaries between attributes of a latent unit in DM-based DRL. DyGA dynamically selects anchors for attribute clusters in the latent space and shifts ambiguous points at the cluster boundaries toward these anchors. This well-organized attribute latent unit is used as a condition for the DM, learning to simultaneously perform disentanglement of the feature extractor and image generation of the DM.

However, since DM can also be trained unconditionally, it may ignore unstable latent units during early training and rely less on the feature extractor. This is due to the peculiarity of DM structures which receive the latent unit only as an auxiliary condition via U-Net’s cross-attention; a new aspect that does not need to be considered in variational autoencoder-based DRL methods [22, 31] where the latent

unit is the sole input condition. Ideally, for the diffusion denoising U-Net and feature extractor to learn complementarily, the training should be guided so that, rather than the noisy image input, the latent unit input determines the core image elements.

Therefore, we also propose **Skip Dropout (SD)**, an effective technique that make DM networks more DRL-friendly with a simple adjustment. SD drops U-Net’s skip connection features from the noisy image input, ensuring that the DM training focuses on the latent unit features and the feature extractor, which are the key to disentanglement. In conclusion, through comprehensive modeling for both the latent unit semantics and DM structure, our proposed methods present the potential of DM for more interpretable disentanglement.

Contributions. Our main contributions are as follows:

- We design *Dynamic Gaussian Anchoring*, a novel inductive bias for interpretable disentanglement that guides attribute-separated latent units through anchoring-based manipulation in the latent space.
- We propose *Skip Dropout*, a modification of the U-Net architecture to enhance the disentangling functionality of the feature extractor within the DM-based DRL framework.
- Our techniques have been applied to existing DM-based methods, achieving SOTA unsupervised DRL performance, and the obtained representations demonstrate strengths in downstream tasks as well.

2. Related Work

Disentangled Representation Learning. Disentangled representation learning (DRL) aims to identify underlying factors from observable data, with variational autoencoders (VAEs) initially favored as generative models because their decoders generate exclusively using the information-rich latent space. β -VAE [22] and AnnealVAE [7], for instance, use regularization and information bottleneck principles for this purpose. InfoVAE [74] and FactorVAE [31] focus on mutual information and total correlation, respectively. However, such regularizations alone are insufficient for unsupervised DRL, as explicit inductive bias has been proven to be mandatory for both models and data sets [39]. In response, QLAE [24] introduces learnable latent quantization to promote an organized latent space, providing an inductive bias for meaningful and consistent representations. Tripod [25] suggests a quantization method with finite scalar codebooks after identifying the limitations of latent quantization learning [42]. Despite these efforts, VAE-based models face a trade-off between image quality and disentanglement [9, 22, 31]. Consequently, InfoGAN [10] demonstrated that generative adversarial networks (GANs) [18] have informative latent spaces and can achieve disentanglement via the lower bounds of mutual information. Pre-trained GAN-based methods such as LD [62], CF [54], GS [19], and DS [30] have also been explored. However, GANs’

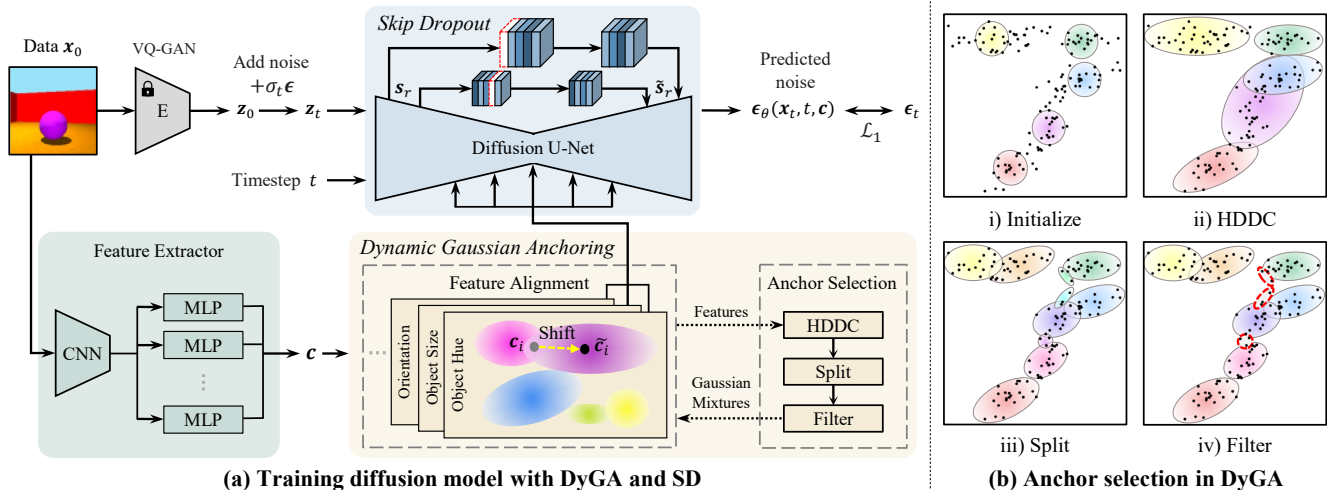


Figure 2. Training framework with proposed methods. (a) During the diffusion model training, the features generated by the feature extractor are shifted towards the mean direction of the Gaussian for each feature unit based on the selected anchor, becoming the condition for the diffusion model. To ensure the diffusion U-Net effectively utilizes the conditions created by the feature extractor, a skip dropout strategy is employed. (b) The process of anchoring Gaussian distributions involves: i) initializing the Gaussian mixture, ii) performing HDDC using the EM algorithm, iii) adjusting the number of Gaussians by splitting them according to criteria, and iv) filtering out unnecessary Gaussians.

instability and mode collapse issues limit their use, leading to recent studies on unsupervised disentanglement with diffusion models [66, 67, 69].

Diffusion Model-based DRL. Due to their generative performance and rich latent space [34], diffusion models have recently gained attention for disentangling their latent space. DisDiff [69] attempted to obtain independent latent vectors using CLUB [11] of mutual information, while FDAE [66] aimed to explicitly improve interpretability by forcing the latent space into separate content and mask codes. Subsequently, EncDiff [67] tried to disentangle the latent space by emphasizing that cross-attention can provide inductive bias through an information bottleneck using only diffusion loss. The general framework, detailed next, establishes a separate feature extractor to derive disentangled representations alongside diffusion model training. However, little has been done to analyze these representations to determine if they truly capture the underlying attributes of each factor. This work delves deeper, introducing a simple yet effective inductive bias for this purpose.

3. Methods

In this section, we begin with a brief explanation of diffusion models. Next, we introduce the overall framework (Sec. 3.1), propose our methodological contributions: (1) Dynamic Gaussian Anchoring as a new inductive bias for diffusion models (Sec. 3.2), and (2) skip dropout to enhance the training of the feature extractor (Sec. 3.3).

Diffusion Models. Diffusion models [23, 28, 51] are a type of latent variable model that reconstruct $x_0 \sim p_{\text{data}}(x_0)$ from

$x_T \sim \mathcal{N}(\mathbf{0}, \mathbf{I})$ with the following formulation $p_\theta(x_0) := \int p_\theta(x_{0:T}) dx_{1:T}$. Diffusion models use a Markov process known as the forward process, which gradually adds noise to the image through a variance schedule β_1, \dots, β_T until it becomes $x_T \sim \mathcal{N}(\mathbf{0}, \mathbf{I})$:

$$q(x_t | x_{t-1}) = \mathcal{N}(x_t; \sqrt{1 - \beta_t}x_{t-1}, \beta_t \mathbf{I}). \quad (1)$$

Then, with $\bar{\alpha}_t = \prod_{s=1}^t \alpha_s$ and $\alpha_t = 1 - \beta_t$, the latent variable x_t at timestep t can be obtained through the following interpolation $x_t = \sqrt{\bar{\alpha}_t}x_0 + \sqrt{1 - \bar{\alpha}_t}\epsilon$, where $\epsilon \sim \mathcal{N}(\mathbf{0}, \mathbf{I})$. This diffusion model optimizes the network according to the following objective:

$$\mathcal{L}_\eta = \mathbb{E}_{x_0, \epsilon, t} [\eta_t || \epsilon_\theta(x_t, t, c) - \epsilon ||], \quad (2)$$

where η_t is the coefficient according to the noise schedule, $\epsilon_\theta(x_t, t, c)$ is the predicted noise, and c is some condition.

3.1. Diffusion Model Framework for DRL

We now introduce our full framework as shown in Fig. 2. Let us first describe the DRL framework involving diffusion models (DM) which is commonly used in recent DM-based DRL methods [66, 67]. Hence, our technical contributions in Sec. 3.2 and Sec. 3.3 can be readily applied to methods based on this framework.

Latent Diffusion Model. Latent diffusion models (LDM) [51] are a type of diffusion model that significantly reduces computational cost by training the diffusion model on images compressed in the latent space rather than the pixel space. LDMs have gained widespread recognition for their utility [45, 53, 72]. We adopt the widely-used LDM framework

with VQ-GAN in order to train conditional generation by conditioning the latent units through cross-attention.

Feature Extractor. The feature extractor extracts a compressed feature from the image, consisting of N latent units. Each latent unit is trained to represent one of the intrinsic factors constituting the image. Similar to previous research [67], the structure of the feature extractor includes a simple CNN that extracts semantic information from the image and an MLP layer applied to each latent unit. Each latent unit is composed of a D -dimensional vector, set to $D = 32$ following prior studies [48, 69]. The entire feature $\mathbf{c} = [\mathbf{c}_1, \dots, \mathbf{c}_N]$, composed of latent units, serves as the condition for the LDM. See the supplement for details.

3.2. Dynamic Gaussian Anchoring

In this subsection, we introduce Dynamic Gaussian Anchoring (DyGA) to ensure that each latent unit of the feature \mathbf{c} faithfully reflects each factor. DyGA is divided into two processes. First, *anchor selection* involves determining the anchors based on the features, with the number of anchors being decided dynamically. Second, *feature alignment* delineates the boundaries between attributes represented by latent units by adjusting the features towards the direction of the selected anchor.

3.2.1 Anchor Selection

As shown in Fig. 2b, anchor selection involves 1) initializing multivariate Gaussian distributions, 2) fitting the Gaussian mixture via high-dimensional data clustering (HDDC) [5], 3) splitting this Gaussians to dynamically increase the number of Gaussians, and 4) filtering out unnecessary Gaussians. At this point, the anchors become the means of the Gaussians, and the splitting and filtering processes serve to dynamically adapt the number of anchors. Meanwhile, HDDC uses the Expectation-Maximization (EM) algorithm to maximize the likelihood function, which is generally non-convex and has many stationary points [40]. This means that HDDC can get trapped in a sub-optimal stationary point. Adjusting the number of anchors provides an opportunity to escape from these stationary points, as it slightly alters the optimization problem. Moreover, it is suitable for unsupervised learning where prior knowledge of the data is unavailable, making it appropriate for cases where the number of attributes within the factors is unknown.

High-dimensional Data Clustering. Finite mixture models [41] predict data distribution as a Gaussian mixture by maximizing the likelihood function through the Expectation-Maximization (EM) algorithm. However, due to the curse of dimensionality [2], this method is difficult to apply to high-dimensional data. To address this, high-dimensional data clustering (HDDC) [5] reduces the high-dimensional problem to a lower-dimensional subspace where the EM update is performed. For Gaussian $\mathcal{N}(\boldsymbol{\mu}_i, \boldsymbol{\Sigma}_i)$, for $i = 1, \dots, K$,

$\boldsymbol{\mu}_i \in \mathbb{R}^d$, and $\boldsymbol{\Sigma}_i \in \mathbb{R}^{d \times d}$, the class conditional covariance matrix $\boldsymbol{\Delta}_i$ is defined as follows:

$$\boldsymbol{\Delta}_i = \mathbf{Q}_i^T \boldsymbol{\Sigma}_i \mathbf{Q}_i, \quad (3)$$

where \mathbf{Q}_i is the orthogonal matrix of eigenvectors of $\boldsymbol{\Sigma}_i$. Consequently, $\boldsymbol{\Delta}_i$ becomes a diagonal matrix with the eigenvalues of $\boldsymbol{\Sigma}_i$ as its diagonal entries. Among these, we let d_i diagonal entries remain unchanged while the remaining $d - d_i$ entries are tied as a single parameter. We can then define the subspace \mathbb{F}_i spanned by d_i eigenvectors and its orthogonal complement $\mathbb{F}_i^\perp \in \mathbb{R}^{d-d_i}$ such that $\mathbb{F}_i \oplus \mathbb{F}_i^\perp = \mathbb{R}^d$. Now, we are able to handle high-dimensional data through a Gaussian mixture model in the subspace \mathbb{F}_i . However, HDDC requires the number of Gaussians to be specified in advance and this number remains fixed. We propose two methods to adjust this dynamically.

Dynamic Adjustment of the Number of Anchors. Gaussians fitted to the features via HDDC represent a stationary point of the likelihood function maximized by the EM algorithm. To address the fact that the optimality of this stationary point cannot be guaranteed [40], there have been attempts to complement this with split/merge strategies in Gaussian mixture models [8, 12, 37]. However, such attempts have not been explored for high-dimensional data. Additionally, a naïve merging strategy may not be suitable for feature alignment, especially when dealing with real-world data where the label may be a continuous value. Therefore, a strategy that dynamically adjusts the number of Gaussians to handle continuous variables is needed.

Gaussian Splitting and Filtering. First, Gaussian splitting is based on the density of the Gaussians according to the responsibility, and the responsibility γ_{ij} of the j -th Gaussian for feature \mathbf{x}_i is given by the following equation:

$$\gamma_{ij} = \frac{\pi_j \mathcal{N}(\mathbf{x}_i | \boldsymbol{\mu}_j, \boldsymbol{\Sigma}_j)}{\sum_{k=1}^K \pi_k \mathcal{N}(\mathbf{x}_i | \boldsymbol{\mu}_k, \boldsymbol{\Sigma}_k)} \quad (4)$$

where π_j is the weight of component j , $\mathcal{N}(\mathbf{x}_i | \boldsymbol{\mu}_j, \boldsymbol{\Sigma}_j)$ is the probability density function (PDF) of the multivariate Gaussian distribution with mean $\boldsymbol{\mu}_j$ and covariance $\boldsymbol{\Sigma}_j$, and these are calculated through EM algorithm. For each Gaussian, the density of the features with a responsibility γ greater than $\phi = 0.5$ (*i.e.*, cluster) is measured. If the density of the fitted Gaussian is higher than $\psi = 0.5$, it is determined that the Gaussian does not adequately reflect the boundaries that need to be disentangled; thus, a split is performed. The density is defined as follows:

$$\text{Density}_i = \frac{1}{N_i} \sum_{j=1}^{N_i} \|\mathbf{x}_{ij} - \frac{1}{N_i} \sum_{k=1}^{N_i} \mathbf{x}_{ik}\|_2 \quad (5)$$

where for cluster i , \mathbf{x}_{ij} is the j -th data point and N_i is the number of data points. In addition, to escape sub-optimal points while covering a large number of attributes, the split is also performed arbitrarily. During every split process, once

a Gaussian is divided into two, it is re-optimized through the EM algorithm using the data belonging to each cluster. After the split process, Gaussian filtering occurs to remove Gaussians that have too few data points in the cluster. This prevents small Gaussians from causing distortions in some features during feature alignment for new data. Re-optimization also occurs after filtering, but since the split and filtering minimally alter the Gaussians, stability remains.

DyGA during the training process. Anchor selection is only possible when there is learned feature data. Therefore, after completing each epoch of training, we use the feature data to select anchors that will be used for future feature alignment. See the supplement for algorithmic details of the entire training process, including anchor selection and feature alignment.

3.2.2 Feature Alignment

Feature alignment refers to the process of shifting a feature $\mathbf{c} = [\mathbf{c}_1, \dots, \mathbf{c}_N]$ towards the mean $\boldsymbol{\mu}_k$ of the Gaussian with the highest responsibility, as described in Eq. (4). Through feature alignment, the boundaries between clusters becomes definite. For $i \in [1, \dots, N]$ and aligned feature $\tilde{\mathbf{c}}_i \in \mathbb{R}^D$, the feature alignment process is as follows:

$$\tilde{\mathbf{c}}_i = \mathbf{c}_i + \delta(\boldsymbol{\mu}_k - \mathbf{c}_i), \quad (6)$$

where $\delta = \lambda \exp\left(-\frac{1}{D} \sum_{j=1}^D \left| \frac{\mathbf{c}_i^j - \boldsymbol{\mu}_k^j}{\mathbf{c}_i^j} \right| \right)$, λ is a scale factor, and the superscript j denotes the j -th element. Since a feature located at the boundary between two Gaussians is sensitive, adjusting this feature is critical to the stability of the diffusion model training. Therefore, fully aligning it to the mean of either Gaussian or using too large λ (e.g., $\lambda \geq 1$) can negatively affect the overall training framework. This could cause the diffusion model to behave as if it were learning unconditional generation. Therefore, as described in Eq. (6), the feature unit $\tilde{\mathbf{c}}_i$ is an interpolation between the feature and the mean $\boldsymbol{\mu}_k$ of the Gaussian. In this process, δ is determined by the distance between the feature and the mean. To prevent excessive variation due to the vector magnitude, δ is bounded by λ , considering the ratio of the difference to the feature. This ensures that the conditional diffusion model can stably utilize the output of the feature extractor, even when the distance from the Gaussian with the highest responsibility is too large. In this paper, $\lambda = 0.1$ was used as the default.

3.3. Skip Dropout

Unlike VAE [7, 22, 32, 74], disentanglement diffusion models [46, 66, 67, 69, 73] are structured with the junction of a feature extractor and the denoising network of a conditional diffusion model. In VAE, the decoder, which is the image generator, depends solely on the latent units. In contrast, the denoising network of the diffusion model relies on

both the flow of the network according to the previous step’s image \mathbf{x}_t and the feature \mathbf{c} . Therefore, during the integrated training process of the diffusion denoising U-Net [52] and the feature extractor, it was necessary to prioritize the training of the feature extractor to achieve DRL-friendly training. Considering this concern, we propose a skip dropout method inspired by DyLoRA [61] as follows:

$$\tilde{\mathbf{s}}_r = \mathbf{s}_r \odot \mathbf{m}, \quad (7)$$

where $\mathbf{m}_i \sim \text{Bernoulli}(p)$, \mathbf{s}_r is the skip connection feature, and $\tilde{\mathbf{s}}_r$ is the dropout-applied skip connection feature.

DyLoRA, inspired by nested dropout [50], uses higher dropout ratios for higher ranks so that the model relies more on lower-rank weights. This implies that dropout [59] can concentrate information on specific weights. We aim to use this property to enhance the feature generation capability of the feature extractor without interfering with the training process of the denoising U-Net. The output of the feature extractor serves as the condition for the diffusion model, which is delivered as keys and values to specific blocks through cross attention. According to FreeU [56] notation, this can be seen as part of the process of forming backbone features. Therefore, we adopt a method to drop out skip connection features at resolutions where conditions are not injected through cross attention, thereby emphasizing the learning of weights that create backbone features (Fig. 2a).

Remark. SD stochastically blinds some of the skip connection feature channels to prevent them from accumulating factor-specific information. As a result, the denoising U-Net yields the learning of the core image information to the feature extractor, which is not connected by skip connections. This allows the feature extractor to be sufficiently trained for disentangled representation.

4. Experiments

Our experiments aimed to verify how effective the proposed DyGA and SD are as inductive biases in the disentanglement of diffusion models. First, we introduce the setup including the dataset and metrics (Sec. 4.1), and then validate the performance by comparing with state-of-the-art models (Sec. 4.2). Additionally, we examine the effectiveness of DyGA and SD in other diffusion-based disentanglement models (Sec. 4.3). We also explore qualitative results through visualization (Sec. 4.4), and validate the performance of each methodology through an ablation study (Sec. 4.5). Subsequently, to evaluate the superiority of our representation, we assess it through a downstream task (Sec. 4.6). For more experiments and analyses, please refer to the supplementary material.

4.1. Experimental Setup

Datasets. We used the datasets Cars3D [47], Shapes3D [6], and MPI3D-toy [17], which are commonly used in disen-

Table 1. Comparison with baselines on the FactorVAE score and DCI disentanglement metrics (mean \pm std). **Bold** indicates the best, and underline indicates the second-best.

Method		Cars3D		Shapes3D		Mpi3D-toy	
		FactorVAE score \uparrow	DCI \uparrow	FactorVAE score \uparrow	DCI \uparrow	FactorVAE score \uparrow	DCI \uparrow
VAE	FactorVAE [31]	0.906 \pm 0.052	0.161 \pm 0.019	0.840 \pm 0.066	0.611 \pm 0.082	0.152 \pm 0.025	0.240 \pm 0.051
	β -TCVAE [9]	0.855 \pm 0.082	0.140 \pm 0.019	0.873 \pm 0.074	0.613 \pm 0.114	0.179 \pm 0.017	0.237 \pm 0.056
	DAVA [16]	0.940 \pm 0.010	0.230 \pm 0.040	0.820 \pm 0.030	0.780 \pm 0.030	0.480 \pm 0.050	0.270 \pm 0.030
GAN	ClosedForm [54]	0.873 \pm 0.036	0.243 \pm 0.048	0.951 \pm 0.021	0.525 \pm 0.078	0.523 \pm 0.056	0.318 \pm 0.014
	GANSpace [19]	0.932 \pm 0.018	0.209 \pm 0.031	0.788 \pm 0.091	0.284 \pm 0.034	0.465 \pm 0.036	0.229 \pm 0.042
	DisCo-GAN [48]	0.855 \pm 0.074	0.271 \pm 0.037	0.877 \pm 0.031	0.708 \pm 0.048	0.371 \pm 0.030	0.292 \pm 0.024
DM	DisDiff-VQ [69]	0.976 \pm 0.018	0.232 \pm 0.019	0.902 \pm 0.043	0.723 \pm 0.013	0.617 \pm 0.070	0.337 \pm 0.057
	FDAE [66]	0.918 \pm 0.027	0.232 \pm 0.418	0.987 \pm 0.023	0.917 \pm 0.038	-	-
	EncDiff [67]	0.773 \pm 0.060	<u>0.279</u> \pm 0.022	<u>0.999</u> \pm 0.000	0.969 \pm 0.030	<u>0.872</u> \pm 0.049	0.685 \pm 0.044
	Ours	<u>0.941</u> \pm 0.002	0.414 \pm 0.013	1.000 \pm 0.000	<u>0.938</u> \pm 0.001	0.930 \pm 0.004	<u>0.627</u> \pm 0.002

tangled representation learning [22, 31, 48, 67–69]. On the other hand, since these datasets do not include real-world data, we supplemented them with the CelebA dataset [38], which contains images of celebrity faces. To be consistent with previous research [9, 31, 67, 69], we resized the images from the CelebA dataset to a resolution of 64×64 .

Implementation Details. We employed LDM [51] as our diffusion model in order to reduce the computational cost while keeping in mind the application to high-resolution data. By using the commonly-utilized VQ-GAN, we mapped the pixel space image to a latent space. For image sampling, we used a 100-step DDIM sampler [58]. To effectively extract features with a low computational burden, we used a simple CNN-based encoder similar to the one used in [67]. All experiments were conducted on a single NVIDIA RTX A6000. See supplement for more details.

Baselines. We compare our method with VAE-based methods—FactorVAE [31], β -TCVAE [9], and DAVA [16]—as well as GAN-based methods—ClosedForm [54], GANSpace [19], and DisCo [48]. Furthermore, we include comparisons with diffusion models-based methods such as DisDiff [69], FDAE [66], and EncDiff [67]. For the CelebA dataset, we also compare against diffusion-based models that have attempted representation learning [46, 64] as baselines.

Evaluation Metrics. To evaluate disentanglement performance, we employed the FactorVAE score [31] and DCI [14] as disentanglement metrics. This aims to understand overall performance by selecting metrics with relatively low covariance, based on a study analyzing the covariance between metrics [39]. For results for additional metrics—MIG [9], Modularity [49], SAP score [33], InfoMEC [24], please refer to the supplementary material. For the CelebA dataset, we measured disentanglement performance and image quality using TAD [70] and Fréchet Inception Distance (FID) [20]. Except for FID, all metrics are measured by reducing the dimensionality of vector-shaped latent units using PCA [13],

Table 2. Comparison of disentanglement and generation quality using the TAD and FID metrics (mean \pm std) on CelebA dataset

Model	TAD \uparrow	FID \downarrow
β -VAE [22]	0.088 \pm 0.043	99.8 \pm 2.4
Diff-AE [46]	0.155 \pm 0.010	22.7 \pm 2.1
InfoDiffusion [64]	0.299 \pm 0.006	23.6 \pm 1.3
DisDiff [69]	0.305 \pm 0.010	18.2 \pm 2.1
EncDiff [67]	0.638 \pm 0.008	14.8 \pm 2.3
Ours	0.954 \pm 0.024	12.0 \pm 1.2

as in previous studies [48, 66, 67, 69].

4.2. Comparison with the State-of-the-art Methods

Here, we compare our proposed method with existing DRL works using quantitative measures.

Results: Cars3D, Shapes3D, and MPI3D-toy. As shown in Table 1, **1)** our method achieved a satisfactory FactorVAE score and the best DCI disentanglement performance on Cars3D. On Shapes3D and MPI3D-toy, it achieved either the best or second best results, and recorded a FactorVAE score of **0.930** on the MPI3D dataset, for which most baselines perform poorly. **2)** EncDiff, which employs a simple CNN encoder within the LDM framework, can be considered our base model. Compared to EncDiff, we observed significant performance improvements on the Cars3D dataset, achieving comparable performance across all other datasets.

Results: CelebA. As shown in Table 2, our method demonstrated a significant performance advantage over all other baselines in terms of TAD metric. This suggests that our modeling is not only effective on synthetic datasets designed for disentanglement (Cars3D, Shapes3D, and MPI3D), but also applicable to real-world datasets. Moreover, our method outperformed existing DM-based models in both TAD and FID with a TAD of **0.954**, suggesting that it overcomes the

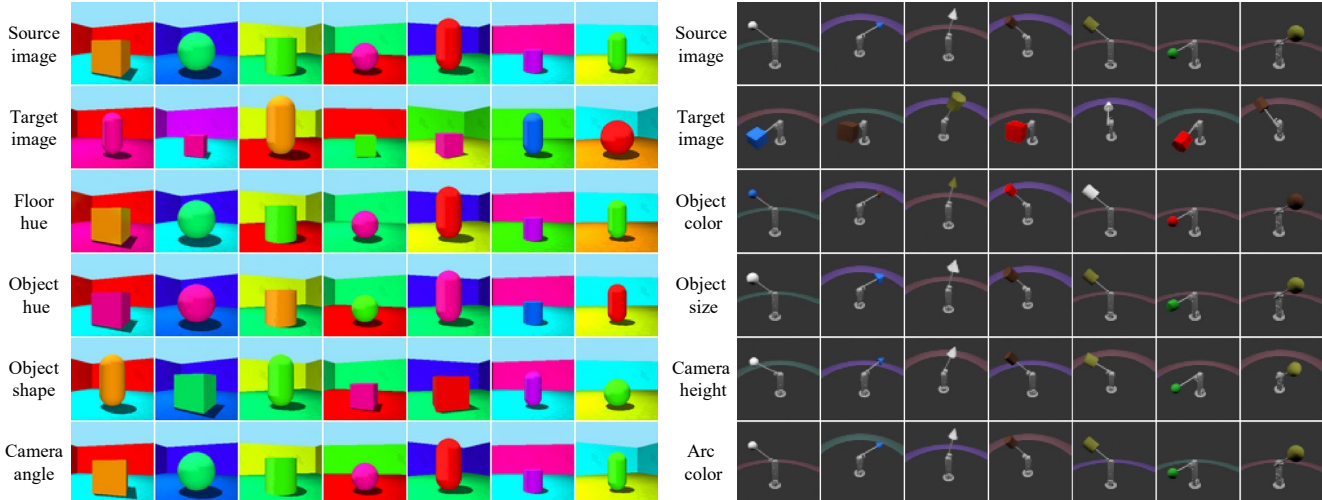


Figure 3. Latent interchange results. This figure shows the results of conditional generation using latent units as the condition, where a single latent unit of the source image is replaced with a latent unit from the target image. The first and second rows represent the source image and target image, respectively. The third to sixth rows show the source image with its attribute (e.g., Floor hue, Camera angle) changed to that of the target. (left) represents the Shapes3D dataset, while (right) represents the MPI3D dataset.

trade-off between image quality and disentanglement, which is a known limitation of VAE-based DRL.

4.3. Application to Other Diffusion Models

Our methods can be plugged into other diffusion model-based DRL architectures where the diffusion models are conditioned on the outputs of any feature extractor. Through an example of combining with DisDiff [69] shown in Table 3, we present that the proposed techniques are effective even when applied to other models.

Since EncDiff uses a LDM and a CNN-based encoder, it allows for an indirect comparison with our method, which is discussed in Sec. 4.2. To verify the effectiveness of our method on another diffusion model, we applied it to DisDiff, which has open source code available. We used the default hyperparameters and set the number of latent units $N = 10$. DyGA was applied to the features passing through the DisDiff encoder, while SD was applied to the skip connection features used by the decoder. As a result, as shown in Table 3, our method proved effective in other DM for DRL contexts as well. This demonstrates that our proposed DyGA and SD not only possess versatility across various models but also serve as effective inductive biases for disentanglement.

4.4. Visualization Results

Latent Interchange Results. A straightforward way to prove whether the trained feature extractor outputs well-disentangled representations is by directly manipulating them. If the visualized results accurately reflect the intended changes in the representation, it means the latent units effectively capture the factors. Here, we refer to changing one of the latent units of a source image to that of a target image as

Table 3. Validation of our method’s effectiveness in DisDiff [69]

Method	Shapes3D		MPI3D-toy	
	FactorVAE score \uparrow	DCI \uparrow	FactorVAE score \uparrow	DCI \uparrow
DisDiff	0.902 \pm 0.043	0.723 \pm 0.013	0.617 \pm 0.070	0.337 \pm 0.057
+DyGA, SD	0.915 \pm 0.027	0.745 \pm 0.018	0.643 \pm 0.057	0.368 \pm 0.060

latent interchange. The image generated using the modified representation as a condition reflects the single latent unit information from the target image onto the source image. As shown in Fig. 3, our method accurately conveys subtle differences, such as camera angle, object color, confirming its effectiveness in altering the image.

Attention Map Visualization. The conditional diffusion model we used injects conditions through the cross-attention layer, allowing for visualization via the corresponding attention map. As shown in Fig. 4, this attention map shows which regions of the image the diffusion U-Net focuses on for noise prediction based on each latent unit. If a latent unit indeed represents a specific factor, the heat map will reflect the regions associated with that factor. We visualized the average of all interpolated attention maps using the method from DAAM [60] in Fig. 4 where it can be seen that the U-Net focuses on the factors represented by each latent unit in the Shapes3D dataset. Meanwhile, in the MPI3D-toy dataset, due to the variety of object orientations, the attention maps cover relatively broader areas, yet still capture the most defining features of the objects. For the camera height, the attention map shows a focus on the gap between the object and the floor as it changes with the camera angle, while also detecting the changes in the position of the arc.

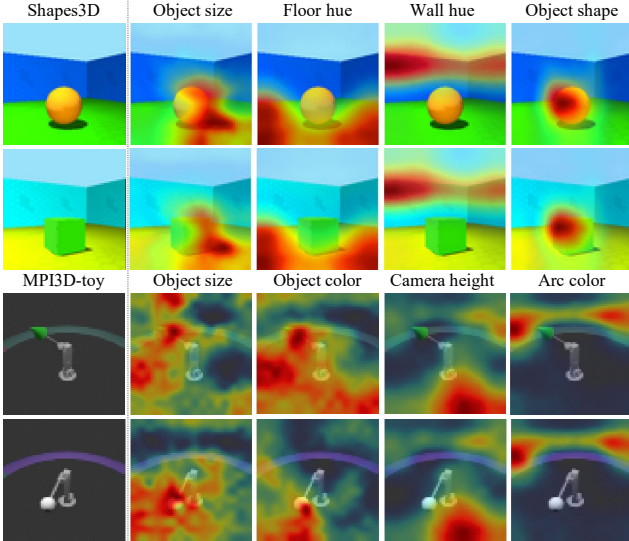


Figure 4. Attention map visualizations on Shapes3D and MPI3D-toy datasets. These results verify how well the image regions highlighted by the attention maps correspond to the factors represented by the latent units. In both datasets, the denoising U-Net focuses on the correct positions associated with the factors represented by the latent units (e.g., object size, object shape).

4.5. Ablation Study

We further analyzed our proposed methods through an ablation study and discussed the results in Table 4. First, we used a LDM with a CNN-based feature extractor as our base model and conducted experiments by applying DyGA and SD separately. The experiments were conducted using the MPI3D-toy dataset, which is sufficiently large and includes both simple elements like color and complex elements such as subtle differences in angle. The experimental results showed that both DyGA and SD individually improved performance in terms of FactorVAE score and DCI disentanglement. When both methods were applied together, the best performance was achieved. Notably, as illustrated in Fig. 1, we observed better attribute alignment within latent units when both methods were applied, and the clearer boundaries between attributes within latent units had a positive impact on performance, as we had anticipated.

4.6. Downstream Tasks

DRL is inherently focused on obtaining useful and meaningful representations within the machine learning domain. In this subsection, we evaluate how much the representation improves learning efficiency by using the gradient boosted trees (GBT). This involves a classification task using the representations, where the two kinds of accuracy Acc_{1000} and Acc_{100} obtained from training with 1000 and 100 representation samples, respectively, are compared to the accuracy

Table 4. Ablation results on the MPI3D-toy dataset

Method	FactorVAE score \uparrow	DCI \uparrow
Baseline	0.856 ± 0.004	0.586 ± 0.002
+DyGA	0.880 ± 0.004	0.626 ± 0.001
+SD	0.863 ± 0.005	0.615 ± 0.002
+DyGA, SD	0.930 ± 0.004	0.627 ± 0.002

Table 5. Statistical efficiency for learning a GBT downstream task on Shapes3D and MPI3D-toy datasets

Method	Shapes3D		MPI3D-toy	
	$\text{Acc}_{1000}/\text{Acc}$	$\text{Acc}_{100}/\text{Acc}$	$\text{Acc}_{1000}/\text{Acc}$	$\text{Acc}_{100}/\text{Acc}$
DisDiff	0.928 ± 0.001	0.732 ± 0.002	0.862 ± 0.001	0.700 ± 0.002
FDAE	0.979 ± 0.002	0.751 ± 0.019	-	-
EncDiff	0.975 ± 0.000	0.772 ± 0.002	0.853 ± 0.005	0.701 ± 0.001
Ours	0.990 ± 0.000	0.863 ± 0.001	0.888 ± 0.002	0.757 ± 0.001

Acc obtained from training 10,000 samples. This serves as a metric to assess how efficient learning is by using fewer samples [39]. To the best of our knowledge, there has been no prior attempts to perform this downstream task on the datasets we used. Therefore, we reproduced the existing models [66, 67, 69] to serve as baselines, using the default hyperparameters suggested in the respective papers. As shown in Table 5, our method outperformed the existing baselines in the downstream tasks for both datasets. The significant improvement in the downstream tasks suggests that the inductive bias that separates attributes within latent units helps obtain better representations.

5. Conclusion

In this study, we propose DyGA and SD, two novel approaches for disentangled representation learning by focusing directly on the latent unit itself. Through empirical evaluation on various datasets, our proposed methods showcase remarkable performance in both disentanglement and downstream tasks. Our DyGA, for the first time, introduces a disentanglement inductive bias which takes into account the attributes of each latent unit. This ensures that each latent unit is interpretable in real-world applications, enhancing their practicality. In addition, our proposed SD transforms the training framework of DMs for DRL into a DRL-friendly approach through stochastic blinding. However, as the number of Gaussians in DyGA is not a continuous variable, the approach has limitations in handling attributes with continuous values. Nonetheless, DyGA can potentially be applied to any dataset, since discrete variables can approximate continuous attributes. In conclusion, our proposed methods emerge as powerful inductive biases for disentangled representation learning, ensuring the fidelity of latent units to reflect factors.

Acknowledgments. This work was supported in part by the IITP RS-2020-II201361 (AI Graduate School Program at Yonsei University), NRF RS-2024-00345806, and NRF RS-2023-00219019 funded by Korean Government (MSIT).

References

- [1] Alyaa Aloraibi. Image morphing techniques: A review. *Technium: Romanian Journal of Applied Sciences and Technology*, 9:41–53, 2023. 16
- [2] Richard Bellman. Dynamic programming. *Chapter IX, Princeton University Press, Princeton, New Jersey*, 1958. 4
- [3] Yoshua Bengio, Aaron Courville, and Pascal Vincent. Representation learning: A review and new perspectives. *IEEE transactions on pattern analysis and machine intelligence*, 35(8):1798–1828, 2013. 1
- [4] Diane Bouchacourt, Ryota Tomioka, and Sebastian Nowozin. Multi-level variational autoencoder: Learning disentangled representations from grouped observations. In *Proceedings of the AAAI Conference on Artificial Intelligence*, volume 32, 2018. 1
- [5] Charles Bouveyron, Stéphane Girard, and Cordelia Schmid. High-dimensional data clustering. *Computational statistics & data analysis*, 52(1):502–519, 2007. 4
- [6] Chris Burgess and Hyunjik Kim. 3d shapes dataset. <https://github.com/deepmind/3dshapes-dataset/>, 2018. 5, 12, 14
- [7] Christopher P Burgess, Irina Higgins, Arka Pal, Loic Matthey, Nick Watters, Guillaume Desjardins, and Alexander Lerchner. Understanding disentangling in beta-vae. *arXiv preprint arXiv:1804.03599*, 2018. 2, 5
- [8] Jason Chang and John W Fisher III. Parallel sampling of dp mixture models using sub-cluster splits. *Advances in Neural Information Processing Systems*, 26, 2013. 4
- [9] Ricky TQ Chen, Xuechen Li, Roger B Grosse, and David K Duvenaud. Isolating sources of disentanglement in variational autoencoders. *Advances in neural information processing systems*, 31, 2018. 2, 6, 15
- [10] Xi Chen, Yan Duan, Rein Houthoofd, John Schulman, Ilya Sutskever, and Pieter Abbeel. Infogan: Interpretable representation learning by information maximizing generative adversarial nets. *Advances in neural information processing systems*, 29, 2016. 2
- [11] Pengyu Cheng, Weituo Hao, Shuyang Dai, Jiachang Liu, Zhe Gan, and Lawrence Carin. Club: A contrastive log-ratio upper bound of mutual information. In *International conference on machine learning*, pages 1779–1788. PMLR, 2020. 3
- [12] Thiago Ferreira Covões, Eduardo Raul Hruschka, and Joydeep Ghosh. Evolving gaussian mixture models with splitting and merging mutation operators. *Evolutionary computation*, 24(2):293–317, 2016. 4
- [13] Yilun Du, Shuang Li, Yash Sharma, Josh Tenenbaum, and Igor Mordatch. Unsupervised learning of compositional energy concepts. *Advances in Neural Information Processing Systems*, 34:15608–15620, 2021. 6
- [14] Cian Eastwood and Christopher KI Williams. A framework for the quantitative evaluation of disentangled representations. In *International conference on learning representations*, 2018. 6, 15
- [15] Patrick Esser, Robin Rombach, and Bjorn Ommer. Taming transformers for high-resolution image synthesis. In *Proceedings of the IEEE/CVF conference on computer vision and pattern recognition*, pages 12873–12883, 2021. 14
- [16] Benjamin Estermann and Roger Wattenhofer. Dava: Disentangling adversarial variational autoencoder. *arXiv preprint arXiv:2303.01384*, 2023. 1, 6
- [17] Muhammad Waleed Gondal, Manuel Wuthrich, Djordje Miladinovic, Francesco Locatello, Martin Breidt, Valentin Volchkov, Joel Akpo, Olivier Bachem, Bernhard Schölkopf, and Stefan Bauer. On the transfer of inductive bias from simulation to the real world: a new disentanglement dataset. *Advances in Neural Information Processing Systems*, 32, 2019. 5, 12, 14
- [18] Ian Goodfellow, Jean Pouget-Abadie, Mehdi Mirza, Bing Xu, David Warde-Farley, Sherjil Ozair, Aaron Courville, and Yoshua Bengio. Generative adversarial nets. *Advances in neural information processing systems*, 27, 2014. 2
- [19] Erik Härkönen, Aaron Hertzmann, Jaakko Lehtinen, and Sylvain Paris. Ganspace: Discovering interpretable gan controls. *Advances in neural information processing systems*, 33:9841–9850, 2020. 2, 6
- [20] Martin Heusel, Hubert Ramsauer, Thomas Unterthiner, Bernhard Nessler, and Sepp Hochreiter. Gans trained by a two time-scale update rule converge to a local nash equilibrium. *Advances in neural information processing systems*, 30, 2017. 6
- [21] Irina Higgins, David Amos, David Pfau, Sebastien Racaniere, Loic Matthey, Danilo Rezende, and Alexander Lerchner. Towards a definition of disentangled representations. *arXiv preprint arXiv:1812.02230*, 2018. 1
- [22] Irina Higgins, Loic Matthey, Arka Pal, Christopher P Burgess, Xavier Glorot, Matthew M Botvinick, Shakir Mohamed, and Alexander Lerchner. beta-vae: Learning basic visual concepts with a constrained variational framework. *ICLR (Poster)*, 3, 2017. 1, 2, 5, 6
- [23] Jonathan Ho, Ajay Jain, and Pieter Abbeel. Denoising diffusion probabilistic models. *Advances in neural information processing systems*, 33:6840–6851, 2020. 1, 3
- [24] Kyle Hsu, William Dorrell, James Whittington, Jiajun Wu, and Chelsea Finn. Disentanglement via latent quantization. *Advances in Neural Information Processing Systems*, 36, 2024. 2, 6, 15
- [25] Kyle Hsu, Jubayer Ibn Hamid, Kaylee Burns, Chelsea Finn, and Jiajun Wu. Tripod: Three complementary inductive biases for disentangled representation learning. *arXiv preprint arXiv:2404.10282*, 2024. 1, 2, 15
- [26] Haiyang Huang, Yingfan Wang, Cynthia Rudin, and Edward P Browne. Towards a comprehensive evaluation of dimension reduction methods for transcriptomic data visualization. *Communications biology*, 5(1):719, 2022. 1
- [27] Eric Jang, Shixiang Gu, and Ben Poole. Categorical reparameterization with gumbel-softmax. *arXiv preprint arXiv:1611.01144*, 2016. 13

- [28] Tero Karras, Miika Aittala, Timo Aila, and Samuli Laine. Elucidating the design space of diffusion-based generative models. *Advances in neural information processing systems*, 35:26565–26577, 2022. [3](#)
- [29] Tero Karras, Miika Aittala, Jaakko Lehtinen, Janne Hellsten, Timo Aila, and Samuli Laine. Analyzing and improving the training dynamics of diffusion models. In *Proceedings of the IEEE/CVF Conference on Computer Vision and Pattern Recognition*, pages 24174–24184, 2024. [1](#)
- [30] Valentin Khruikov, Leyla Mirvakhabova, Ivan Oseledets, and Artem Babenko. Disentangled representations from non-disentangled models. *arXiv preprint arXiv:2102.06204*, 2021. [2](#)
- [31] Hyunjik Kim and Andriy Mnih. Disentangling by factorising. In *International conference on machine learning*, pages 2649–2658. PMLR, 2018. [2](#), [6](#), [15](#)
- [32] Diederik P Kingma and Max Welling. Auto-encoding variational bayes. *arXiv preprint arXiv:1312.6114*, 2013. [5](#), [15](#)
- [33] Abhishek Kumar, Prasanna Sattigeri, and Avinash Balakrishnan. Variational inference of disentangled latent concepts from unlabeled observations. *arXiv preprint arXiv:1711.00848*, 2017. [6](#), [15](#)
- [34] Mingi Kwon, Jaeseok Jeong, and Youngjung Uh. Diffusion models already have a semantic latent space. *arXiv preprint arXiv:2210.10960*, 2022. [2](#), [3](#)
- [35] Brenden M Lake, Tomer D Ullman, Joshua B Tenenbaum, and Samuel J Gershman. Building machines that learn and think like people. *Behavioral and brain sciences*, 40:e253, 2017. [1](#)
- [36] Yann LeCun, Yoshua Bengio, and Geoffrey Hinton. Deep learning. *nature*, 521(7553):436–444, 2015. [1](#)
- [37] Yan Li and Lei Li. A novel split and merge em algorithm for gaussian mixture model. In *2009 Fifth International Conference on Natural Computation*, volume 6, pages 479–483. IEEE, 2009. [4](#)
- [38] Ziwei Liu, Ping Luo, Xiaogang Wang, and Xiaoou Tang. Deep learning face attributes in the wild. In *Proceedings of International Conference on Computer Vision (ICCV)*, December 2015. [6](#), [12](#)
- [39] Francesco Locatello, Stefan Bauer, Mario Lucic, Gunnar Raetsch, Sylvain Gelly, Bernhard Schölkopf, and Olivier Bachem. Challenging common assumptions in the unsupervised learning of disentangled representations. In *international conference on machine learning*, pages 4114–4124. PMLR, 2019. [1](#), [2](#), [6](#), [8](#)
- [40] Geoffrey J McLachlan and Thriyambakam Krishnan. *The EM algorithm and extensions*. John Wiley & Sons, 2007. [4](#)
- [41] Geoffrey J McLachlan and David Peel. *Finite mixture models*, volume 299. John Wiley & Sons, 2000. [4](#)
- [42] Fabian Mentzer, David Minnen, Eirikur Agustsson, and Michael Tschannen. Finite scalar quantization: Vq-vae made simple. *arXiv preprint arXiv:2309.15505*, 2023. [2](#), [15](#)
- [43] Nathan Michlo, Richard Klein, and Steven James. Overlooked implications of the reconstruction loss for vae disentanglement. *arXiv preprint arXiv:2202.13341*, 2022. [1](#)
- [44] Jonas Peters, Dominik Janzing, and Bernhard Schölkopf. *Elements of causal inference: foundations and learning algorithms*. The MIT Press, 2017. [1](#)
- [45] Dustin Podell, Zion English, Kyle Lacey, Andreas Blattmann, Tim Dockhorn, Jonas Müller, Joe Penna, and Robin Rombach. Sdxl: Improving latent diffusion models for high-resolution image synthesis. *arXiv preprint arXiv:2307.01952*, 2023. [3](#)
- [46] Konpat Preechakul, Nattanat Chatthee, Suttisak Widadwongsa, and Supasorn Suwajanakorn. Diffusion autoencoders: Toward a meaningful and decodable representation. In *Proceedings of the IEEE/CVF Conference on Computer Vision and Pattern Recognition*, pages 10619–10629, 2022. [5](#), [6](#)
- [47] Scott E Reed, Yi Zhang, Yuting Zhang, and Honglak Lee. Deep visual analogy-making. *Advances in neural information processing systems*, 28, 2015. [5](#), [12](#), [14](#)
- [48] Xuanchi Ren, Tao Yang, Yuwang Wang, and Wenjun Zeng. Learning disentangled representation by exploiting pretrained generative models: A contrastive learning view. *arXiv preprint arXiv:2102.10543*, 2021. [1](#), [4](#), [6](#)
- [49] Karl Ridgeway and Michael C Mozer. Learning deep disentangled embeddings with the f-statistic loss. *Advances in neural information processing systems*, 31, 2018. [6](#), [15](#)
- [50] Oren Rippel, Michael Gelbart, and Ryan Adams. Learning ordered representations with nested dropout. In *International Conference on Machine Learning*, pages 1746–1754. PMLR, 2014. [5](#)
- [51] Robin Rombach, Andreas Blattmann, Dominik Lorenz, Patrick Esser, and Björn Ommer. High-resolution image synthesis with latent diffusion models. In *Proceedings of the IEEE/CVF conference on computer vision and pattern recognition*, pages 10684–10695, 2022. [1](#), [3](#), [6](#), [14](#)
- [52] Olaf Ronneberger, Philipp Fischer, and Thomas Brox. U-net: Convolutional networks for biomedical image segmentation. In *Medical image computing and computer-assisted intervention—MICCAI 2015: 18th international conference, Munich, Germany, October 5–9, 2015, proceedings, part III 18*, pages 234–241. Springer, 2015. [5](#)
- [53] Nataniel Ruiz, Yuanzhen Li, Varun Jampani, Yael Pritch, Michael Rubinstein, and Kfir Aberman. Dreambooth: Fine tuning text-to-image diffusion models for subject-driven generation. In *Proceedings of the IEEE/CVF conference on computer vision and pattern recognition*, pages 22500–22510, 2023. [3](#)
- [54] Yujun Shen and Bolei Zhou. Closed-form factorization of latent semantics in gans. In *Proceedings of the IEEE/CVF conference on computer vision and pattern recognition*, pages 1532–1540, 2021. [2](#), [6](#)
- [55] Ken Shoemake. Animating rotation with quaternion curves. In *Proceedings of the 12th annual conference on Computer graphics and interactive techniques*, pages 245–254, 1985. [16](#)
- [56] Chenyang Si, Ziqi Huang, Yuming Jiang, and Ziwei Liu. Freeu: Free lunch in diffusion u-net. In *Proceedings of the IEEE/CVF Conference on Computer Vision and Pattern Recognition*, pages 4733–4743, 2024. [5](#)
- [57] Krishna Kumar Singh, Utkarsh Ojha, and Yong Jae Lee. Finegan: Unsupervised hierarchical disentanglement for fine-grained object generation and discovery. In *Proceedings of*

- the *IEEE/CVF conference on computer vision and pattern recognition*, pages 6490–6499, 2019. [1](#)
- [58] Jiaming Song, Chenlin Meng, and Stefano Ermon. Denoising diffusion implicit models. *arXiv preprint arXiv:2010.02502*, 2020. [6](#)
- [59] Nitish Srivastava, Geoffrey Hinton, Alex Krizhevsky, Ilya Sutskever, and Ruslan Salakhutdinov. Dropout: a simple way to prevent neural networks from overfitting. *The journal of machine learning research*, 15(1):1929–1958, 2014. [5](#), [16](#)
- [60] Raphael Tang, Linqing Liu, Akshat Pandey, Zhiying Jiang, Gefei Yang, Karun Kumar, Pontus Stenetorp, Jimmy Lin, and Ferhan Ture. What the daam: Interpreting stable diffusion using cross attention. *arXiv preprint arXiv:2210.04885*, 2022. [7](#)
- [61] Mojtaba Valipour, Mehdi Rezagholizadeh, Ivan Kobzyev, and Ali Ghodsi. Dylora: Parameter efficient tuning of pre-trained models using dynamic search-free low-rank adaptation. *arXiv preprint arXiv:2210.07558*, 2022. [5](#)
- [62] Andrey Voynov and Artem Babenko. Unsupervised discovery of interpretable directions in the gan latent space. In *International conference on machine learning*, pages 9786–9796. PMLR, 2020. [2](#)
- [63] Xin Wang, Hong Chen, Si’ao Tang, Zihao Wu, and Wenwu Zhu. Disentangled representation learning. *arXiv preprint arXiv:2211.11695*, 2022. [1](#)
- [64] Yingheng Wang, Yair Schiff, Aaron Gokaslan, Weishen Pan, Fei Wang, Christopher De Sa, and Volodymyr Kuleshov. Infodiffusion: Representation learning using information maximizing diffusion models. In *International Conference on Machine Learning*, pages 36336–36354. PMLR, 2023. [6](#)
- [65] George Wolberg. Image morphing: a survey. *The Visual Computer*, 14:360–372, 1998. [16](#)
- [66] Ancong Wu and Wei-Shi Zheng. Factorized diffusion autoencoder for unsupervised disentangled representation learning. 2024. [1](#), [2](#), [3](#), [5](#), [6](#), [8](#), [14](#)
- [67] Tao Yang, Cuiling Lan, Yan Lu, et al. Diffusion model with cross attention as an inductive bias for disentanglement. *arXiv preprint arXiv:2402.09712*, 2024. [1](#), [2](#), [3](#), [4](#), [5](#), [6](#), [8](#), [14](#)
- [68] Tao Yang, Yuwang Wang, Yan Lu, and Nanning Zheng. Visual concepts tokenization. *NeurIPS*, 2022. [6](#)
- [69] Tao Yang, Yuwang Wang, Yan Lv, and Nanning Zheng. Disdiff: Unsupervised disentanglement of diffusion probabilistic models. *arXiv preprint arXiv:2301.13721*, 2023. [1](#), [2](#), [3](#), [4](#), [5](#), [6](#), [7](#), [8](#)
- [70] Eric Yeats, Frank Liu, David Womble, and Hai Li. Nashae: Disentangling representations through adversarial covariance minimization. In *European Conference on Computer Vision*, pages 36–51. Springer, 2022. [6](#)
- [71] Kaiwen Zhang, Yifan Zhou, Xudong Xu, Bo Dai, and Xingang Pan. Diffmorpher: Unleashing the capability of diffusion models for image morphing. In *Proceedings of the IEEE/CVF Conference on Computer Vision and Pattern Recognition*, pages 7912–7921, 2024. [16](#)
- [72] Lvmin Zhang, Anyi Rao, and Maneesh Agrawala. Adding conditional control to text-to-image diffusion models. In *Proceedings of the IEEE/CVF International Conference on Computer Vision*, pages 3836–3847, 2023. [3](#)
- [73] Zijian Zhang, Zhou Zhao, and Zhijie Lin. Unsupervised representation learning from pre-trained diffusion probabilistic models. *Advances in neural information processing systems*, 35:22117–22130, 2022. [5](#)
- [74] Shengjia Zhao, Jiaming Song, and Stefano Ermon. InfoVAE: Information maximizing variational autoencoders. *arXiv preprint arXiv:1706.02262*, 2017. [2](#), [5](#)
- [75] Bhushan Zope and Soniya B. Zope. A survey of morphing techniques. *International Journal of Advanced engineering, Management and Science*, 3:81–87, 2017. [16](#)

A. Additional Materials

An overview of the paper and a brief presentation video are available on our project page: <https://youngjun-jun.github.io/dis-dis-rep>.

B. Datasets

This section provides an overview of the benchmark datasets (Fig. 5). The number of samples for each dataset is shown in Table 6.

Cars3D [47]. The Cars3D dataset is a car dataset created from CAD models with the following ground truth factors: elevation, azimuth, object type.

Shapes3D [6]. The Shapes3D dataset is composed of 3D shapes with the following ground truth factors: floor hue, wall hue, object hue, scale, shape, orientation.

MPI3D-toy [17]. The MPI3D-toy dataset is part of the MPI3D dataset created to benchmark representation learning in simulated and real-world environments. It focuses on the toy type with the following ground truth factors: object color, object shape, object size, camera height, background color, first DOF, second DOF.

CelebA [38]. The CelebFaces Attributes Dataset (CelebA) is a face attributes dataset with 40 attributes. Although CelebA is not specifically designed for disentanglement, it allows for the validation of effects in real-world scenarios using various attributes.

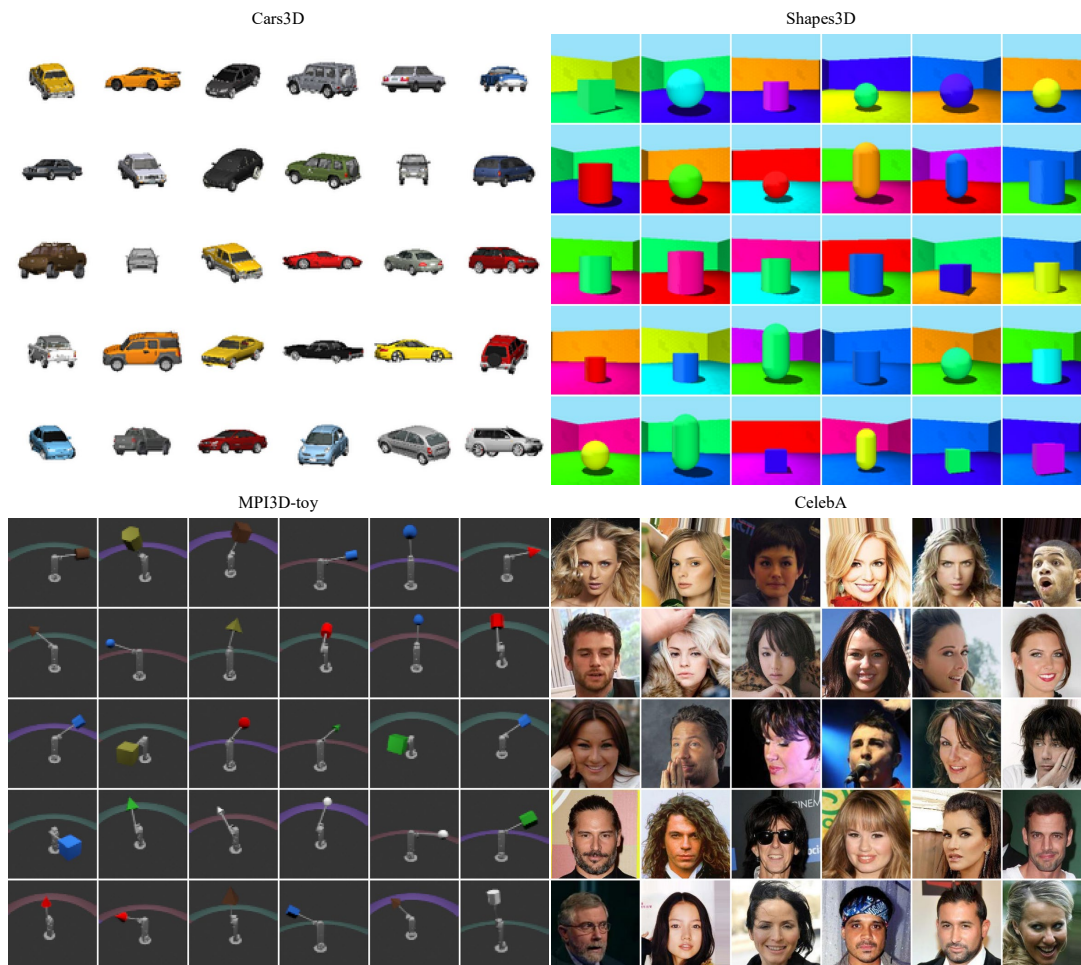


Figure 5. The samples from each dataset

Table 6. The number of samples for each dataset

Cars3D	Shapes3D	MPI3D	CelebA
17,568	480,000	1,036,000	202,599

C. More Implementation Details

C.1. Training Details

C.1.1 Algorithms

Entire training framework. As in Algorithm 1, the LDM training process using DyGA is conducted on an epoch-by-epoch basis. After every r epochs, *anchor selection* is performed for *feature alignment* in the subsequent r epochs. Considering the dataset size, we set $r = 5$ for the Cars3D dataset, while $r = 1$ was used for the others.

Anchor selection in DyGA. The anchor selection process (Algorithm 2) consists of four stages. First, subspaces are updated using HDDC. Then, a Gaussian to split is selected based on density, and the two split Gaussians are updated using only the features within the cluster. Next, excessively small Gaussians that could act as outliers during feature alignment are removed. Finally, the Gaussians are updated using HDDC. These steps are performed at the latent unit level, with multi-processing utilized for each latent unit and accelerated through matrix multiplication. The anchor selection process for a single latent unit is completed within 30 seconds.

Feature alignment in DyGA. Naïvely aligning features with the anchors selected through anchor selection hinders the backpropagation process. Therefore, as shown in Algorithm 3, we use the Gumbel-softmax function [27] with a sufficiently small $\tau = 0.0001$ to prevent distortion of the Gaussian mean while still allowing back-propagation. After this, the features undergo alignment in the direction of the anchor.

Algorithm 1 Entire training framework

Input: \mathbf{X} : dataset, $\{\sigma_t\}_{t=1}^T$: Noise schedule, $E(\cdot)$: VQ-encoder, $\epsilon_\theta(\cdot)$: Denoising network, $f(\cdot)$: Feature extractor

for $epoch = 1, \dots, max_epoch$ **do**

for $\mathbf{x}_0^i \in \mathbf{X}$ **do**

 Sample $\epsilon \sim \mathcal{N}(\mathbf{0}, \mathbf{I})$, $t \sim \text{Uniform}(\{0, 1, \dots, T\})$

$\mathbf{z}_t^i \leftarrow E(\mathbf{x}_0^i) + \sigma_t \epsilon$

$\mathbf{c}_i \leftarrow f(\mathbf{x}_0^i)$

if $epoch \geq r$ **then** $\tilde{\mathbf{c}}_i \leftarrow \text{Feature_alignment}(\mathbf{c}_i)$

else $\tilde{\mathbf{c}}_i \leftarrow \mathbf{c}_i$

end if

 Predict noise $\epsilon_\theta(\mathbf{z}_t, t, \tilde{\mathbf{c}}_i)$

 Compute loss and gradient

 Update parameters θ

Anchor_selection

end for

end for

Algorithm 2 Anchor selection of the k^{th} cluster

Input: $\mathbf{c} \in \mathbb{R}^d$: latent units
Output: $\mu_k, \Sigma_k, w_k, \Lambda_k, \mathbf{v}_k, D_k$
Initialize $\mu_k, \Sigma_k, w_k, \Lambda_k, \mathbf{v}_k, D_k$
for $iter = 1, \dots, max_iter$ **do**
 E-step: Calculate r_{ik}
 M-step: Update μ_k, Σ_k, w_k
 Update subspaces: Compute $\Lambda_k, \mathbf{v}_k, D_k$
end for
Calculate density of clusters $\in \mathcal{F}$
while $\mathcal{F} \neq \emptyset$ **do**
 Choose cluster $\mathbf{f} \in \mathcal{F}$
 Split cluster \mathbf{f}
 E-step, M-step, and Update subspaces in the *cluster*
 Update \mathcal{F}
end while
Remove small Gaussians
for $iter = 1, \dots, max_iter$ **do**
 E-step, M-step, and Update subspaces
end for

Algorithm 3 Feature alignment

Input: $\mathbf{c} \in \mathbb{R}^d$: latent unit, τ : softmax parameter, λ : feature alignment parameter
Output: $\hat{\mathbf{c}} \in \mathbb{R}^d$
E-step: Calculate responsibility r
Gumbel-Softmax:
 1. Generate Gumbel noise g_k
 2. Compute $y_k = \text{softmax}\left(\frac{r_k + g_k}{\tau}\right)$
Update $\mu_k \leftarrow \sum_k y_k \mu_k$
Compute multiplier $\delta \leftarrow \lambda \exp\left(-\frac{1}{d} \sum_{j=1}^d \left| \frac{\mathbf{c}_i^j - \mu_k^j}{\mathbf{c}^j} \right| \right)$
Align latent unit $\tilde{\mathbf{c}} \leftarrow \mathbf{c} + \delta(\mu_k - \mathbf{c})$

C.1.2 LDM training details

During the training process of LDM, we set the batch size to 512 for the Cars3D [47], Shapes3D [6], and MPI3D-toy [17] datasets, and 64 for the CelebA dataset. The learning rate and Exponential Moving Average (EMA) rate were set to 0.0001 and 0.9999, respectively, for all datasets, following EncDiff [67].

C.2. Model Architecture

The latent diffusion model (LDM) [51] we used is a diffusion model for images in the latent space reduced by VQ-GAN [15]. The architectures of VQ-GAN and the LDM denoising U-Net are shown in Table 7 and Table 8, respectively. Additionally, the feature extractor (Table 9), similar to previous studies [66, 67], uses a structure where a scalar value is taken for each latent unit through a CNN module and then passed through independent MLP modules. We used the same settings for all datasets.

Table 7. VQ-GAN architecture parameters

Parameter	Value
Embedding dimensionality	3
Number of embeddings	2048
Channels in first conv layer	32
Channel multipliers	[1, 2, 4]
Residual blocks per layer	2
Dropout rate	0.0
Discriminator start epoch	0
Discriminator loss weight	0.75
Codebook loss weight	1.0

Table 8. Denoising U-Net architecture parameters

Parameter	Value
Input image size	16
Input channels	3
Base channels	64
Attention resolutions	[1, 2, 4]
Residual blocks per layer	2
Channel multipliers	[1, 2, 4, 4]
Attention heads	8
Scale-shift normalization	True
Context dimension	32
Dropout rate	0.1
Skip dropout rate	0.2
Noise schedule	Linear
Diffusion timestep	1000

Table 9. Feature extractor architecture

CNN module
Conv $7 \times 7 \times 3 \times 64$, stride= 1, padding= 3
BatchNorm
ReLU
Conv $4 \times 4 \times 64 \times 128$, stride= 1, padding= 3
BatchNorm
ReLU
Conv $4 \times 4 \times 128 \times 256$, stride= 2, padding= 1
BatchNorm
ReLU
Conv $4 \times 4 \times 256 \times 256$, stride= 2, padding= 1
BatchNorm
ReLU
Conv $4 \times 4 \times 256 \times 256$, stride= 2, padding= 1
BatchNorm
ReLU
FC 4096×4096
ReLU
FC 4096×256
ReLU
FC $256 \times N$
MLP module
FC 1×256
ReLU
FC 256×512
ReLU
FC 512×32
ReLU

D. More Experiments

D.1. Results for more metrics

In this subsection, as shown in Table 10, we evaluate the disentanglement performance of our method using not only the FactorVAE score [31] and DCI disentanglement [14], but also additional metrics such as MIG [9], Modularity score [49], SAP score [33], and InfoMEC InfoM score [24].

Table 10. Results for more metrics on Cars3D, Shapes3D and MPI3D-toy datasets

Dataset	FactorVAE score \uparrow	DCI \uparrow	MIG \uparrow	Modularity score \uparrow	SAP score \uparrow	InfoM score \uparrow
Cars3D	0.941 ± 0.002	0.414 ± 0.013	0.109 ± 0.002	0.934 ± 0.001	0.009 ± 0.002	0.417 ± 0.004
Shapes3D	1.000 ± 0.000	0.938 ± 0.001	0.507 ± 0.002	0.930 ± 0.001	0.183 ± 0.006	0.569 ± 0.002
MPI3D-toy	0.930 ± 0.004	0.627 ± 0.002	0.364 ± 0.001	0.882 ± 0.002	0.174 ± 0.002	0.495 ± 0.003

D.2. DyGA and SD Analysis

DyGA Analysis. Our proposed *Dynamic Gaussian Anchoring* (DyGA) can dynamically adjust the position and number of anchors. A similar approach can be found in the quantization methods used in variational autoencoder (VAE) [32]-based approaches [24, 25]. One such method, finite scalar quantization (FSQ) [42], can be applied to diffusion-based models as a way to organize latent units. However, when we set the number of codebooks to 1 and the levels to [8, 5, 5], performance

Table 11. Comparison between DyGA and FSQ

Method	FactorVAE score \uparrow	DCI \uparrow
Baseline	0.856 \pm 0.004	0.586 \pm 0.002
+FSQ, SD	0.606 \pm 0.006	0.384 \pm 0.002
+DyGA, SD	0.930 \pm 0.004	0.627 \pm 0.002

actually degraded, as shown in Table 6, with similar performance drops observed in other settings. This suggests that attempts to organize latent units in diffusion-based models using a fixed number of quantization values or fixed quantized values may not be suitable. Therefore, we introduced DyGA, which dynamically adjusts the number and positions of anchors, resulting in significant performance improvements.

Table 12. Skip and Backbone Dropout

Method	FactorVAE score \uparrow	DCI \uparrow
+BD-0.1	0.798 \pm 0.005	0.610 \pm 0.002
Baseline	0.856 \pm 0.004	0.586 \pm 0.002
+SD-0.1	0.852 \pm 0.005	0.598 \pm 0.007
+SD-0.2	0.863 \pm 0.005	0.615 \pm 0.002
+SD-0.3	0.855 \pm 0.006	0.603 \pm 0.002

SD Analysis. *Skip Dropout* (SD) stochastically blinds skip connection features to prevent the continuous accumulation of factor information in specific weights. This forces the diffusion U-Net to rely on the backbone features connected to the feature extractor, which continuously provide factor information. To analyze this effect more deeply, we examine the impact of SD by using backbone dropout (BD), which dropouts backbone features in parts with skip connections. On the other hand, it has been shown that dropout rates between 0.4 and 0.8 do not affect performance improvement [59], and we have experimentally found that a high skip dropout ratio (*e.g.*, $1 - p = 1.0$) negatively impacts the convergence of the diffusion model. Therefore, we used skip dropout rates of 0.1, 0.2, and 0.3, while the backbone dropout rate was set to 0.1. As a result, as shown in Table 12, an appropriate skip dropout rate was effective, whereas backbone dropout degraded performance.

D.3. Latent Interpolation

There has been no exploration of the disentangled representation space of diffusion-based models (*i.e.*, the space of outputs from the feature extractor). In this subsection, we visualize images generated by interpolating latent units extracted from two images. This intermediate image generation enables image morphing [1, 65, 71, 75], which shows the transformation between images as a video. Experimentally, when using spherical linear interpolation (slerp) [55] for the diffusion latent interpolation method in DiffMorpher [71], the generated intermediate images appeared unnatural. Instead, as shown in Fig. 6, images generated using linear interpolation suggest the potential for image morphing through disentanglement.

E. More Visualizations

E.1. Training loss curve

In this subsection, we plot the training loss curve according to different parameters. From Fig. 7, we can confirm that our methods remain stable despite changes in training parameters (λ : feature alignment parameter, $1 - p$: skip dropout ratio).

E.2. More Latent Interchange Results

One way to verify if a trained feature extractor extracts well-disentangled representations is to manipulate them directly. If the visualized results accurately reflect the intended changes in representation, it indicates that the latent units faithfully represent the factors. Here, we refer to changing one of the latent units of the source image to the latent unit of the target image as a latent interchange. The images generated using the latent units created through latent interchange conditionally alter the source image using the single latent unit information of the target image. Fig. 8 visualizes how well the feature extractor is

trained in each dataset through latent interchange. Our method demonstrates that the images generated using latent interchange effectively reflect a single characteristic of the target image.

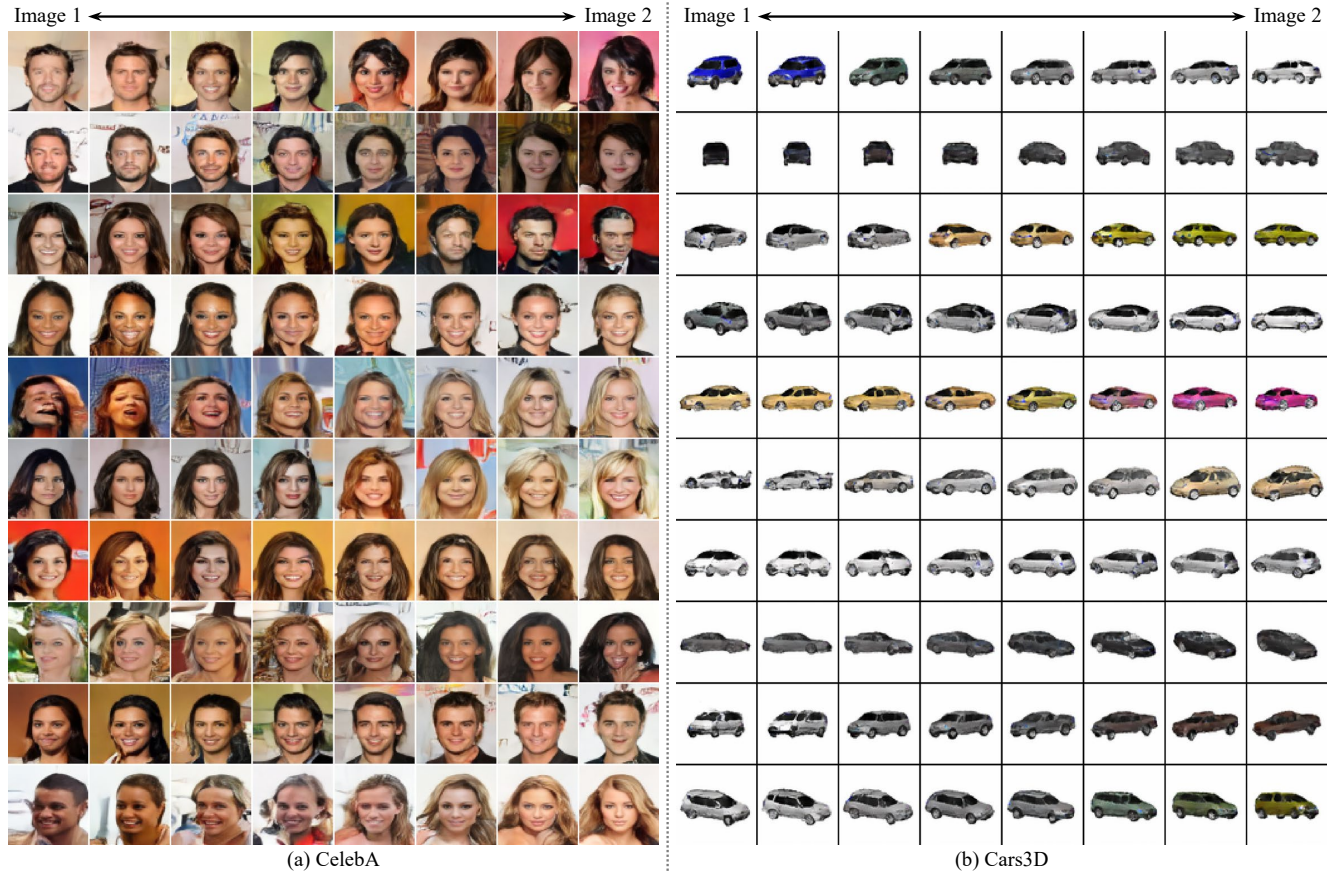


Figure 6. Visualization of latent interpolation on the Cars3D and CelebA datasets. (a) For CelebA, we observe natural transitions between two images in terms of hair color, hair style, skin color, background color, gender, and smile. (b) Similarly, in Cars3D, we observe smooth changes in vehicle type, color, azimuth, and elevation.

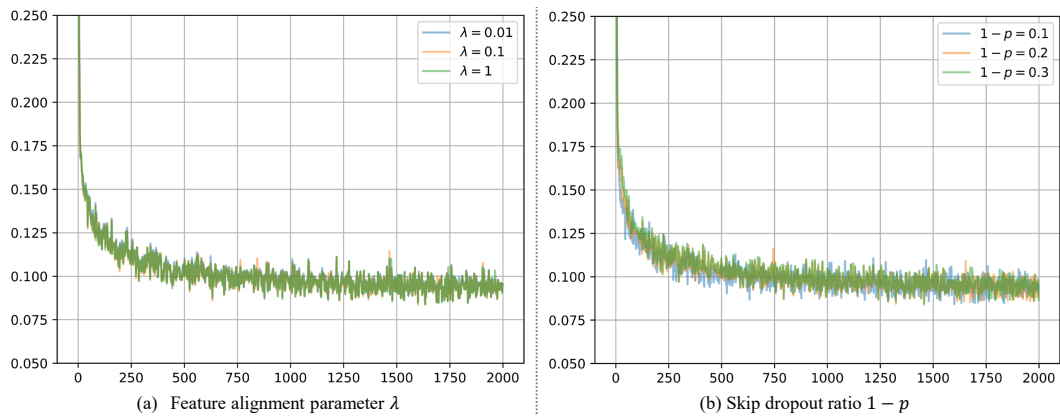


Figure 7. Training loss curve

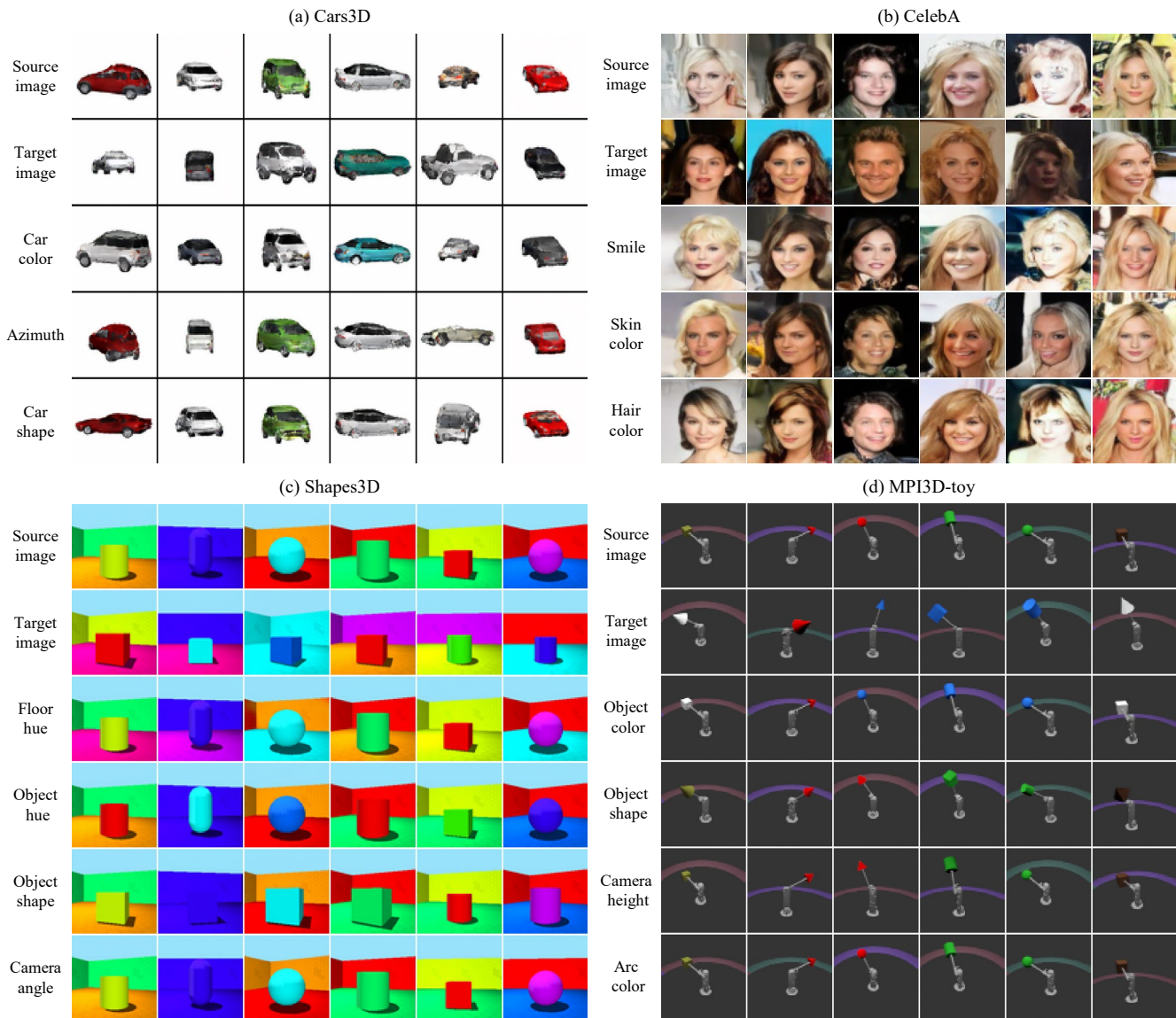


Figure 8. Latent interchange results on Cars3D, Shapes3D, MPI3D-toy, and CelebA datasets

E.3. More Attention Map Visualizations

Since our diffusion model receives conditions through cross attention, it is possible to visualize the attention map. This attention map shows which areas of the image are being highlighted, indicating which parts of the image each latent unit uses to generate. The results on various datasets can be seen in Figs. 9 and 10.

E.4. More Latent Unit Visualizations

Disentangled representation learning aims to make each latent unit sensitive to a single fundamental factor while being invariant to the other factors. At this point, the latent unit with the highest association (*e.g.*, normalized mutual information) to a given factor best reflects the information of that factor. Therefore, we visualize the latent units for various data points in the Shapes3D dataset (Fig. 11) to see how well the latent units separate the factor attributes.

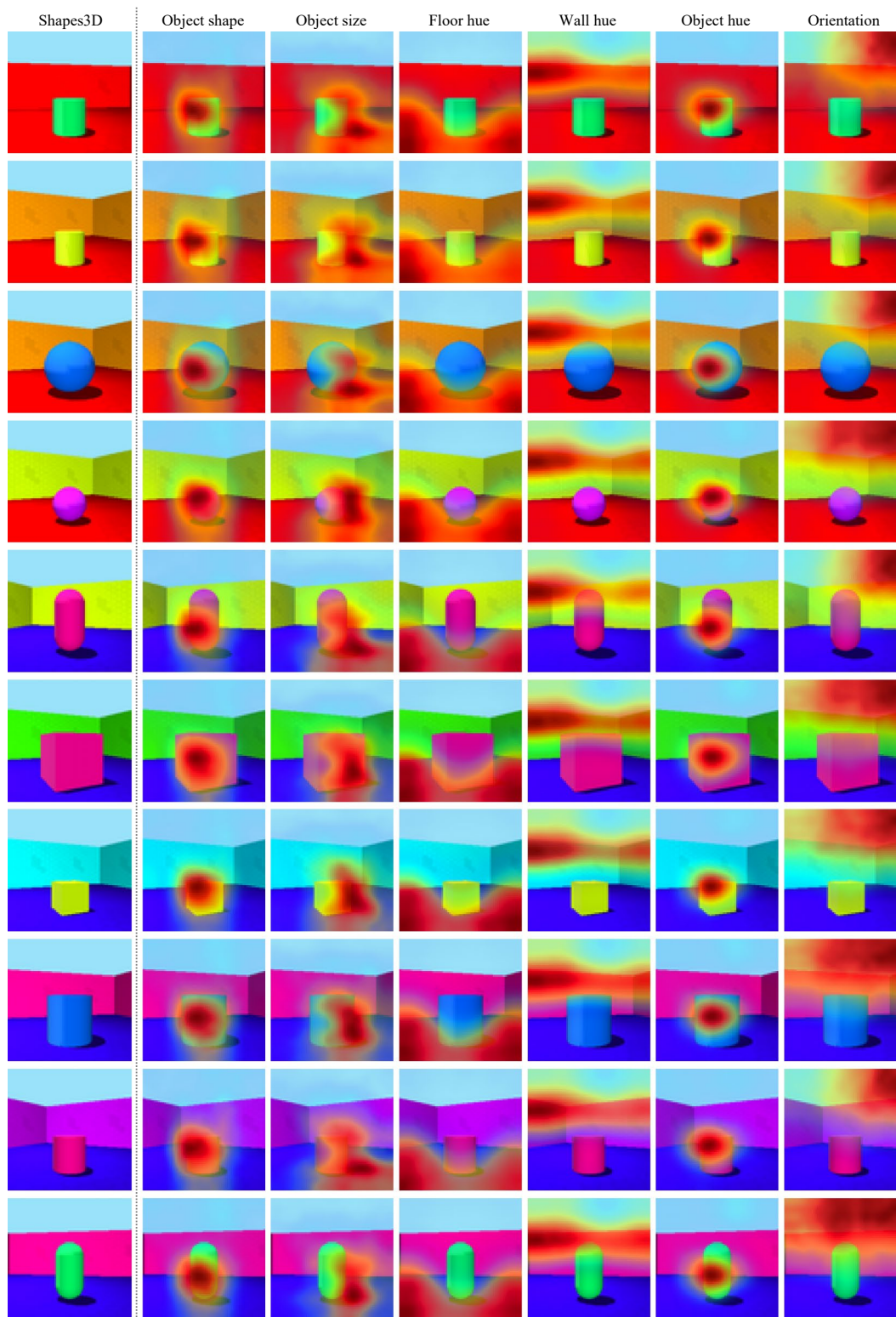


Figure 9. Attention map visualizations on Shapes3D dataset

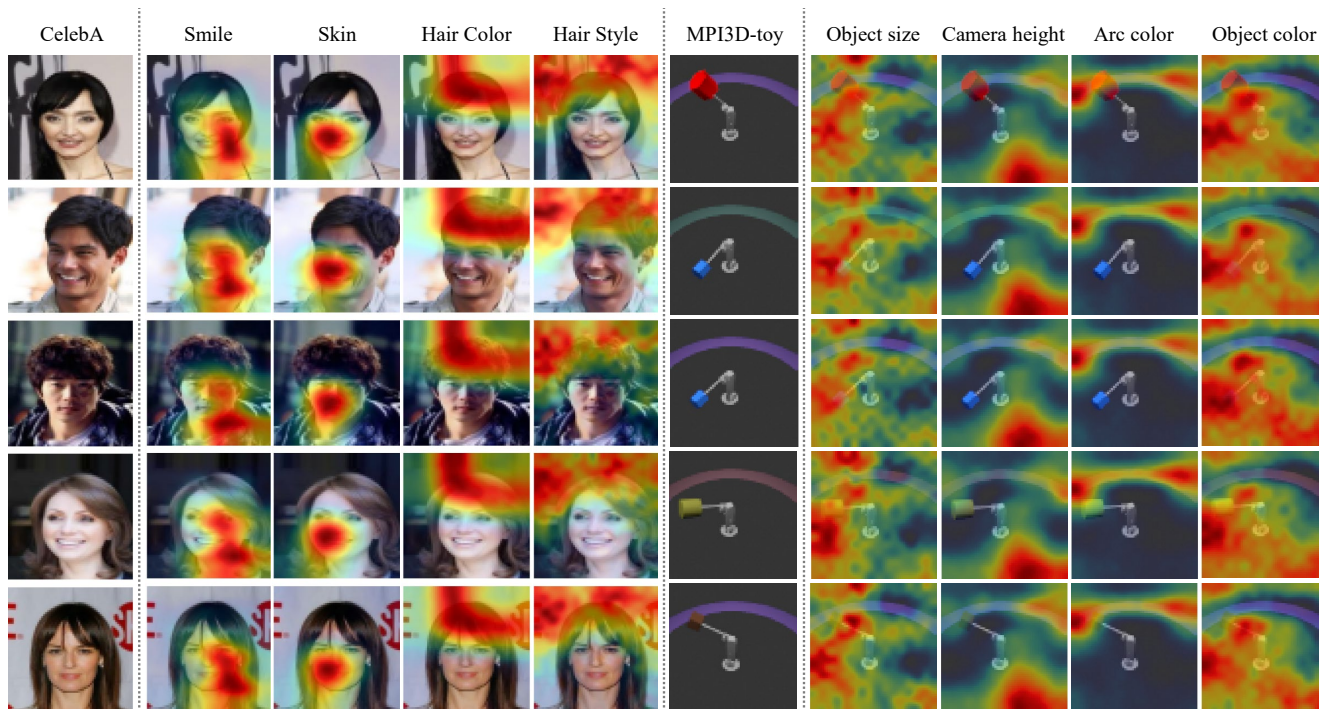


Figure 10. Attention map visualizations on CelebA and MPI3D-toy datasets

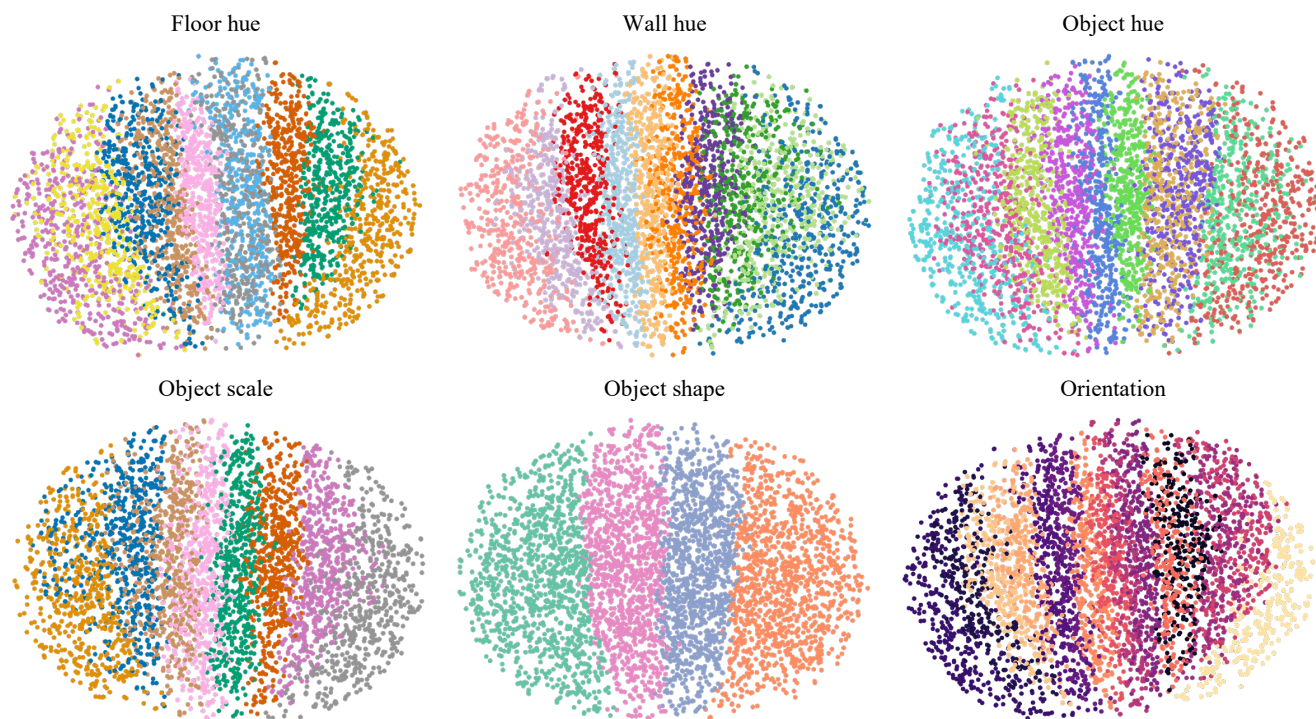


Figure 11. Visualization of latent units on Shapes3D dataset. Each visualized latent unit here is associated with the written factor (*e.g.*, it has the highest normalized mutual information). Each color represents an attribute of the factor, such as *red* in object color or *cube* in object shape.